ELSEVIER

Contents lists available at ScienceDirect

Journal of Non-Crystalline Solids

journal homepage: www.elsevier.com/locate/jnoncrysol



New insights into the structure of sodium silicate glasses by force-enhanced atomic refinement



Qi Zhou^a, Tao Du^{a,b,c}, Lijie Guo^{d,*}, Morten M. Smedskjaer^e, Mathieu Bauchy^{a,*}

- ^a Physics of AmoRphous and Inorganic Solids Laboratory (PARISlab), Department of Civil and Environmental Engineering, University of California, Los Angeles CA 90095, USA
- b Key Lab of Structures Dynamic Behavior and Control (Harbin Institute of Technology), Ministry of Education, 150090 Harbin, China
- ^c School of Civil Engineering, Harbin Institute of Technology, Harbin 150090, China
- ^d National Centre for International Research on Green Metal Mining, BGRIMM Technology Group, Beijing 100160, China
- e Department of Chemistry and Bioscience, Aalborg University, Aalborg 9220, Denmark

ARTICLE INFO

Keywords: Silicate glasses Atomic structure Medium-range order Molecular dynamics Reverse Monte Carlo modeling

ABSTRACT

Atomistic simulations can offer direct access to the atomic structure of glasses, which is otherwise invisible from conventional experiments. However, molecular dynamics (MD) simulations of glasses based on the meltquenching technique remain plagued by the use of high cooling rates, while reverse Monte Carlo (RMC) modeling can yield non-unique solutions. Here, we adopt the force-enhanced atomic refinement (FEAR) method to overcome these limitations and decipher the atomic structure of a sodium silicate glass. We show that FEAR offers an unprecedented description of the atomic structure of sodium silicate, wherein the simulated configuration simultaneously exhibits enhanced agreement with experimental diffraction data and higher energetic stability as compared to those generated by MD or RMC. This result allows us to reveal new insights into the atomic structure of sodium silicate glasses. Specifically, we show that sodium silicate glasses exhibit a more ordered medium-range order structure than previously suggested by MD simulations. These results pave the way toward an increased ability to accurately describe the atomic structure of glasses.

1. Introduction and background

Despite their critical role in various technological applications (e.g., optical fibers, display application, nuclear waste immobilization, etc.), the atomic structure of silicate glasses remains only partially understood [1–5]. This is largely due to the fact that, although conventional experiments (e.g., nuclear magnetic resonance, neutron or X-ray diffraction, etc.) offer useful "fingerprints" of the glass structure (e.g., pair distribution function, coordination numbers, etc.), they do not provide direct access to the atomic structure itself (i.e., the cartesian positions of the atoms). Indeed, although experimental data offer important constraints on the glass structure, these constraints cannot uniquely define the structure itself. For instance, a virtually infinite number of very different structures can present the same pair distribution function [6], so that the full and detailed atomic structure of a glass cannot be uniquely inverted from the mere knowledge of experimental data [7].

As an alternative, complementary route, atomistic simulations offer a direct and full access to the atomic structure of glasses [8–10]. However, atomistic simulations remain plagued by several intrinsic

limitations. As a first option, MD simulations are usually based on the melt-quench (MQ) method, wherein a melt is equilibrated at high temperature to lose the memory of its initial configuration and subsequently cooled down to the glassy state [11]. The time-dependent positions of the atoms are then computed by numerically solving Newton's law of motion based on the knowledge of the interatomic forcefield. Although the MQ method mimics the usual experimental synthesis protocol of glasses, most of the MQ-MD simulations are limited to very small timescales (a few ns) due to their computational cost [12]. Hence, MD simulations based on the MQ method are intrinsically limited to cooling rates (typically around 1 K/ps) that are several orders of magnitude higher than experimental ones [9,13-16]. This is a serious drawback for out-of-equilibrium glasses, as their structure and properties depend on the thermal history [17–20]. As such, due to the use of high cooling rates, MQ-MD simulations usually tend to overestimate the glass fictive temperature and, hence, to yield glass structures that are more disordered than those observed experimentally [9,21]. As a second option, RMC simulations have been used to "invert" available experimental data into atomic structures, that is, to generate some

E-mail addresses: ljguo264@126.com, guolijie@bgrimm.com (L. Guo), bauchy@ucla.edu (M. Bauchy).

^{*} Corresponding authors.

atomic structures satisfying given experimental constraints [6,22–24]. However, despite their apparent success (since the structure of RMC-based glasses will necessarily exhibit an excellent agreement with experimental data), RMC simulations are intrinsically based on an ill-defined problem, since, as mentioned above, several glass structure can present the same experimental fingerprint—so that a glass structure cannot be uniquely inverted from experimental data [25]. Although hybrid RMC (HRMC) approaches comprising an energy penalty term have been proposed [26–28], the choice of the weights associated with experimental constraints and energy penalty during the refinement remains partially arbitrary. Altogether, these limitations have raised doubts regarding the ability of atomistic simulations to offer a realistic description of the atomic structure of glasses and, thus, of their properties.

Recently, Drabold et al. introduced a new "information-driven" paradigm, wherein the knowledge of both experimental constraints and the interatomic forcefield is simultaneously leveraged to produce realistic atomic models of glasses [29]. Specially, Drabold et al. proposed a force-enhanced atomic refinement (FEAR) method, which relies on an iterative combination of RMC refinements (i.e., based on available experimental constraints) and energy minimizations (i.e., based on the knowledge of the interatomic forcefield) [7,29,30]. Unlike alternative hybrid RMC approaches—wherein both structure and energy are optimized simultaneously-the interatomic forces are here only computed during the energy minimization steps, which results in an improved overall computational efficiency [29]. In addition, the FEAR method does not rely on any assumption regarding the weight attributed to structure and energy during the optimization. This method was shown to yield disordered Si and SiO₂ atomic structures that simultaneously (i) exhibit an excellent agreement with diffraction data and (ii) are more energetically-stable than those obtained by MD simulations relying on the MO method [29].

Here, we adopt the FEAR method to refine the structure of a sodium silicate glass—an archetypal model system for more complex, multicomponent silicate glasses [31]. We show that the FEAR method yields a glass structure that simultaneously exhibits enhanced agreement with neutron diffraction data and higher energetic stability as compared to configurations generated by MQ-MD or RMC, while remaining computationally efficient. Based on these results, we find that the mediumrange order structure of sodium silicate glasses is more ordered than previously suggested by MQ-MD and RMC simulations.

2. Simulations details

2.1. Molecular dynamics simulations

To compare the outcomes of MQ-MD, RMC, HRMC, and FEAR, we simulate a sodium silicate glass (Na₂O)₃₀(SiO₂)₇₀ (mol.%). The system comprises 3000 atoms, which has been found sufficient to describe the atomic structure of silicate glasses [32]. We adopt the well-established Teter forcefield, which has been shown to offer a good description of the structural, mechanical, and dynamical properties of sodium silicate glasses [10,31,33-40]. Based on previous studies, a short-range repulsive term is added to avoid the "Buckingham catastrophe" at high temperature [10]. Cutoff values of 8 and 12 Å are used for the shortrange and Coulombic interactions, respectively [9,31]. The long-range Coulombic interactions are evaluated with the Particle-Particle-Mesh (PPPM) algorithm with an accuracy of 10^{-5} [41]. Note that the PPPM approach relies on the particle mesh method, wherein the particles are interpolated onto a three-dimensional grid. All simulations are carried out using the Large-scale Atomic/Molecular Massively Parallel Simulator (LAMMPS) package [42]. An initial sodium silicate configuration used for the melt-quench method is created by randomly placing the atoms in a cubic box while ensuring the absence of any unrealistic overlap. The system is then melted at 4000 K under zero pressure in the isothermal-isobaric (NPT) ensemble for 100 ps to ensure the complete loss of the memory of the initial configuration. The melt is then linearly cooled down to 0 K under zero pressure in the *NPT* ensemble with a cooling rate of ranging from 100 down to 0.001 K/ps. Note that, although these values remain several orders of magnitude larger than experimental cooling rates, the cooling rate of 0.001 K/ps corresponds to a total simulation time of 4 μ s, which, to the best of our knowledge, is the longest MD simulation conducted for a silicate glass thus far [9,43]. The use of such a slow cooling rate provides us with a reliable reference atomic structure that can be compared with that yielded by FEAR.

2.2. Reverse Monte Carlo simulations

The structure of the same silicate glass is then refined by RMC simulation, as implemented via an in-house fix in LAMMPS [42]. To this end, we use as an experimental constraint the pair distribution function (PDF) obtained from neutron diffraction [44]. The neutron PDF is computed from the partial PDFs $g_{ii}(r)$ as:

$$g_X(r) = \frac{1}{\sum_{i,j=1}^n c_i c_j b_i b_j} \sum_{i,j=1}^n c_i c_j b_i b_j g_{ij}(r),$$
(1)

where c_i are the molar fractions of element i (i = Si, Na, or O) and b_i are the neutron scattering lengths of the species (given by 4.1491, 3.63 and 5.803 fm for Si, Na, and O atoms, respectively) [45]. Note that, to enable a meaningful comparison between simulated and experimental PDFs, the simulated PDF needs to be broadened, which has been traditionally ignored in previous RMC studies. Here, this is achieved by convoluting the computed PDF with a normalized Gaussian distribution with a full width at half-maximum (FWHM) given by FWHM = 5.437/ $Q_{\rm max}$ [46], where $Q_{\rm max}$ is the maximum wave vector used in the diffraction test (here, $Q_{\rm max}$ = 22.88 \mathring{A}^{-1}). The level of agreement between the simulated and experimental PDF is then captured by the R_χ factor proposed by Wright:

$$R_{\chi}^{2} = \sum_{i} [g^{\exp}(r_{i}) - g^{\sin}(r_{i})]^{2} / \left(\sum_{i} g^{\exp}(r_{i})\right)^{2}$$
(2)

The R_χ factor is here calculated from r=0-to-8 Å. The RMC method then consists in the following steps. (i) Starting from a "random" initial configuration, the pair distribution function of the simulated structure is computed and the Wright's coefficient $R_\chi^{\rm old}$ is calculated (see Eq. (2)). (ii) An atom is randomly selected and displaced with a random direction and distance. (iii) The pair distribution function of the new configuration and the new cost function $R_\chi^{\rm new}$ are computed. (iv) Following the Metropolis algorithm, the new configuration is accepted if $R_\chi^{\rm new} \leq R_\chi^{\rm old}$, that is, if the level of agreement between simulated and experimental structure is enhanced by the Monte Carlo move. Otherwise, the atomic displacement is accepted with the following probability or refused otherwise:

$$P = \exp\left[-\frac{R_{\chi}^{\text{new}^2} - R_{\chi}^{\text{old}^2}}{T_{\chi}}\right] \tag{3}$$

where T_χ is a constant that controls the probability of acceptance (that is, higher values of T_χ result in higher probability of acceptance of the Monte Carlo move). Note that the T_χ constant plays the role of an effective (unitless) temperature, since the term $(R_\chi^{\rm new^2}-R_\chi^{\rm old^2})/T_\chi$ is equivalent to the quantity $(U^{\rm new}-U^{\rm old})/(kT)$ in the conventional Metropolis algorithm (where U is the energy of the system). Here, the Wright's coefficient R_χ plays the role of energy (i.e., the metric to be minimized) and T_χ plays the role of a temperature (i.e., which controls the propensity to accept moves that increase R_χ) [22]. Here, we use $T_\chi=0.001$, which was found to result in the lowest final R_χ upon convergence. Atomic displacements and directions are randomly chosen, with a uniform displacement probability distribution between 0 and 0.2 Å. The simulation box size is kept fixed throughout the simulation at L=34.47 Å so that molar volume is fixed according to the

experimental value of $24.7 \text{ cm}^3/\text{mol}$ [47]. A total number of 500,000 RMC moves are attempted until convergence.

2.3. Hybrid reverse Monte Carlo simulations

As a comparison to the traditional RMC method, we then assess the potential benefit of including an energy penalty in the acceptance probability of the Monte Carlo moves. To this, we adopt the HRMC approach proposed by Bousige et al. [27]. Starting from the original RMC approach, this approach alters the probability of acceptance of the Monte Carlo moves by incorporating the variation of the potential energy ΔU as follows:

$$P = \exp\left[-\frac{(R_{\chi}^{\text{new}^2} - R_{\chi}^{\text{old}^2}) + \frac{\Delta U}{\omega}}{T_{\chi}}\right]$$
(4)

where ω is a parameter that governs the relative weight between the penalties associated to the variations of energy and R_χ , namely, (i) $\omega \to \infty$ is equivalent to a pure RMC refinement, while (ii) $\omega \to 0$ is equivalent to a conventional Monte Carlo Metropolis simulation (i.e., wherein the probability of acceptance of the Monte Carlo moves is solely based on the variation of energy). Here, several values of ω are tried so as to eventually achieve the lowest energy and R_χ at the end of the refinement. In the following, we use the following optimized parameters: $T_\chi = 0.01$ and $\omega = 10^{-4}$ eV. A total of 500,000 HRMC moves are attempted until convergence is observed.

2.4. Force-enhanced atomic refinement (FEAR) simulations

Finally, we compare for the same sodium silicate composition the outcomes of the MQ-MD, RMC, and HRMC simulations with the results offered by FEAR, as implemented via an in-house fix in LAMMPS [42]. To this end, we start from a "randomized" structure generated by RMC while using a large fictive temperature, namely, $T_{\chi}=3000$. Following the original implementation of the FEAR method [29], the system is then iteratively subjected to a combination of RMC refinements and energy minimizations, wherein each FEAR iteration consists in (i) 5000 RMC steps and (ii) an energy minimization conducted with the conjugate gradient method. As a refinement of the original method [29], we here subject the system to a volume relaxation every 10 iterations, wherein the simulation box is deformed in order to simultaneously reach minimum energy and zero pressure [48,49]. In the following, all properties referring to the FEAR refinement are averaged over 10 independent runs and error bars are evaluated based on the standard deviations. In addition, we dynamically adjust the selectivity of the Metropolis acceptance criterion by linearly decreasing the effective temperature T_{χ} from 10^3 down to 10^{-6} during the course of the FEAR refinement. These parameters were found to yield a glass structure exhibiting minimum R_{γ} and potential energy values.

3. Results and discussion

3.1. Evolution of the structure upon force-enhanced refinement

Fig. 1 shows selected snapshots of the atomic structure of the simulated sodium silicate glass upon FEAR refinement. Overall, we observe that the degree of connectivity increases upon refinement, which manifests itself by the formation of Si—O bonds. Fig. 2 shows the evolution of the neutron PDF of the simulated sodium silicate glass after selected number of iterations of FEAR refinement. The first peak around 1.6 Å arises from Si—O correlations, while the second peak captures second-neighbors (Si—Si and O—O) correlations [50]. We observe that the peak positions of the initial PDF are in fairly good agreement with experimental neutron diffraction data, which indicates that the initial structure exhibits reasonable inter-atomic distances. However, the intensities of the peaks are initially not well reproduced. In contrast, the

first peak of the PDF of the intermediate structure (after 30 FEAR iterations) shows an excellent agreement with neutron diffraction data—both in terms of position and intensity—whereas the peaks at larger distance remain less refined. This signals that the refinement of the short-range order occurs faster than that of the medium-range order, likely arising from the fact that refining the short-range order only involves some slight displacements of the neighbors of each atom. In contrast, refining of the medium-range order requires some collective atomic displacements, as well as the breakage and formation of interatomic bonds (which requires larger energy barriers to be overcome). Eventually, we find that the PDF of the final configuration exhibits an excellent agreement with neutron data, both for the short- and medium-range order. Notably, the configuration exhibits a Wright R_χ factor of about 2.49% (see Fig. 3a). Note that a threshold R_χ factor of 10% is typically used to discriminate "good" from "bad" structures [46].

3.2. Comparison with molecular dynamics and reverse Monte Carlo

We now compare the outcomes of FEAR refinement with those of MQ-MD, RMC, and HRMC simulations. As shown in Fig. 3a, we first note that, upon RMC refinement, the R_{γ} factor of the simulated sodium silicate glass monotonically decreases and eventually reaches a final R_{γ} value of 1.2%, which highlights an excellent agreement with neutron diffraction data (see Figs. 3b and c). This is not surprising since RMC refinement solely aims to decrease R_{γ} . A similar trend is observed for HRMC refinement—although the final value of R_{γ} is not as low as that offered by RMC and FEAR. This can be understood from the fact that the cost function in HRMC does not only depend on the pair distribution function but also on the energy constraint, so that, for every step during the refinement, there is always a competition between structure and energy. We note that, although RMC eventually yields a lower R_{γ} factor than FEAR and HRMC, RMC requires a few more iterations than FEAR and HRMC to converge. This shows that incorporating a constraint on the energy during the refinement effectively accelerates the refinement. Overall, FEAR exhibits the best balance between final accuracy and computational efficiency.

X-ray diffraction (XRD) offers an additional reference to compare FEAR with RMC, HRMC, and MQ-MD. Indeed, although it is based on the same structural information as the neutron PDF, the XRD PDF places a difference weight on each partial pair distribution function and is not explicitly used during the FEAR, RMC, and HRMC refinement. As shown in Fig. 4, we find that the analysis of the XRD PDF echoes that of the neutron PDF, namely, (i) RMC and FEAR offer the highest accuracy, (ii) HRMC shows a slightly higher R_χ value (but less than 10%), and (iii) the XRD PDF obtained from MQ-MD exhibits more pronounced deviations from the experimental reference—especially at large distance. Overall, these results once again demonstrate that the structures obtained by FEAR and RMC show the best agreement with diffraction data.

To further assess the reliability of the structures predicted by FEAR, RMC, HRMC, and MQ-MD, we now focus on the neutron structure factor, which is computed from the Fourier transform of the neutron pair distribution function (see Ref. [9]). Indeed, although the structure factor contains the same information as the PDF, it places higher emphasis on the structural correlations at longer distances and, hence, can also be used to further characterize the medium-range order. In addition, it offers an additional check to assess the quality of the FEAR refinement, since, unlike the PDF, the structure factor is not explicitly taken into account during the refinement.

Fig. 5 shows the structure factor computed from the FEAR, RMC, HRMC, and MQ-MD configurations. We first find that MD yields a very reasonable description of the structure factor, since all the peaks are fairly well reproduced (see Fig. 4a). In detail, we find that the high-Q region of the structure factor ($Q > 4 \ \mathring{A}^{-1}$) of the glass generated by melt-quenching, which confirms that MD yields a good description of

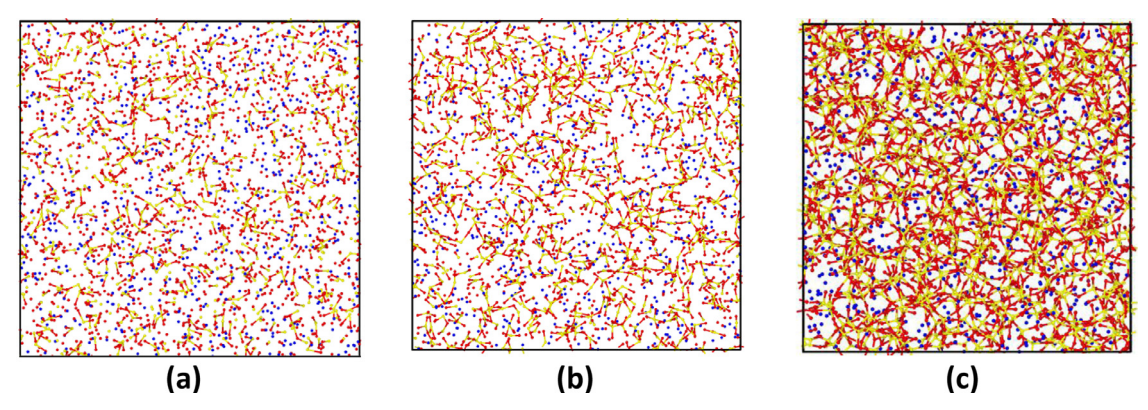


Fig. 1. Snapshots of the (a) initial, (b) intermediate (30 iterations), and (c) final (100 iterations, i.e., at convergence) configurations of the simulated sodium silicate glass upon force-enhanced atomic refinement. The bonds correspond to Si–O pairs that are closer than 2 Å from each other.

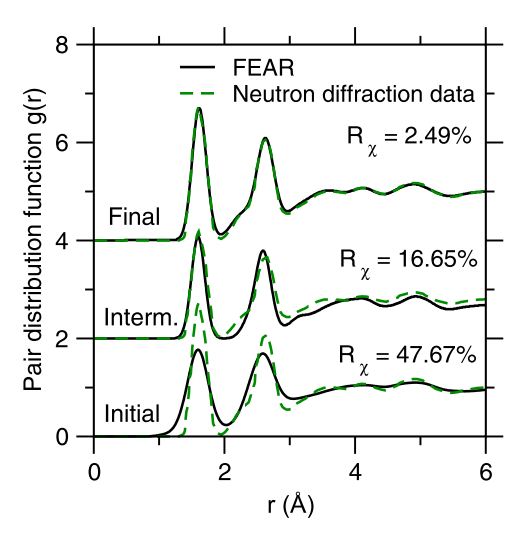


Fig. 2. Computed neutron pair distribution function upon force-enhanced atomic refinement—obtained from the configurations presented in Fig. 1. The data are compared with experimental neutron diffraction data [44].

the short-range order of the glass (see Fig. 3b). Nevertheless, we observe some discrepancies between neutron diffraction data and MD in the low-Q region of the structure factor. In particular, the sharpness and degree of asymmetry of the first-sharp diffraction peak (FSDP) around 2 \mathring{A}^{-1} is not well predicted by MD. This signals that MD offers a fairly poor description of the medium-range order structure of the glass.

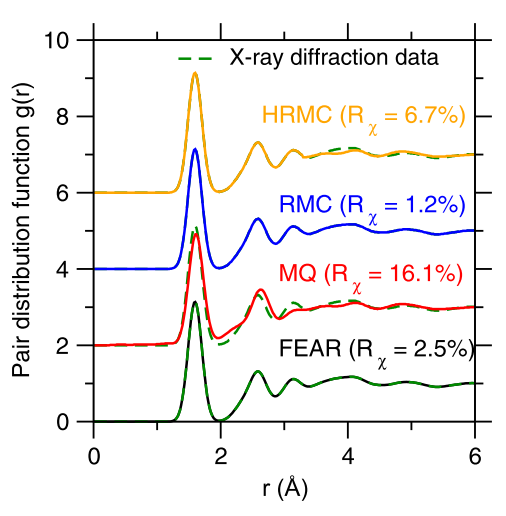


Fig. 4. X-ray pair distribution functions computed by FEAR, MQ, RMC, and HRMC. The data are compared with experimental X-ray diffraction data [51].

In contrast, we find that RMC, HRMC, and FEAR refinements all yield a significantly improved description of the low-Q region of the structure factor—albeit to a higher extent in the case of RMC (see Figs. 5b, c, and d). Importantly, we observe that the position, intensity, sharpness, and asymmetry of the FSDP are very well reproduced by RMC, HRMC, and FEAR refinements. Eventually, we find that RMC, HRMC, and FEAR refinements offer an R_χ factor (calculated, this time,

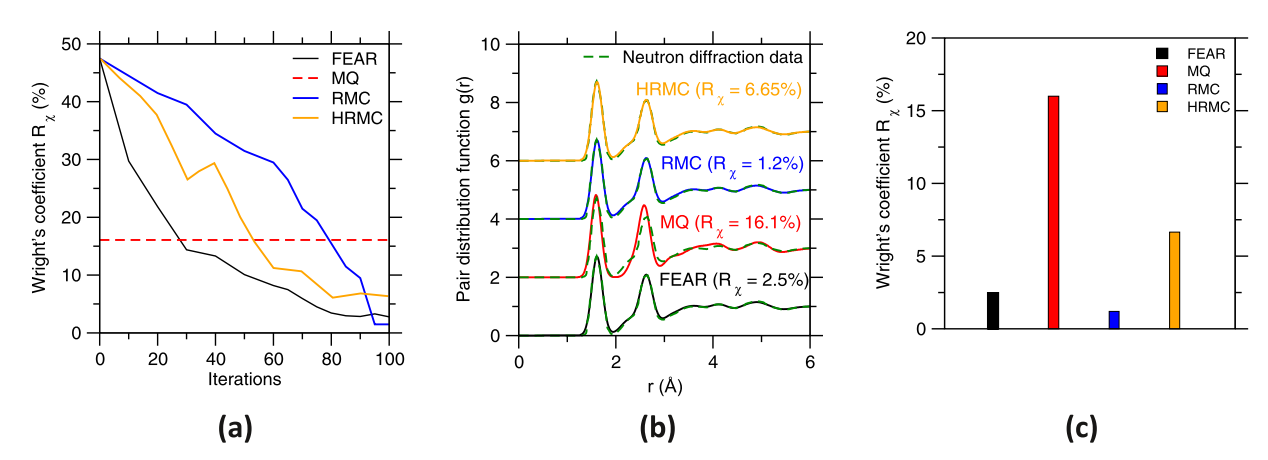


Fig. 3. (a) Wright's coefficient R_χ as a function of the iteration number upon force-enhanced atomic refinement (FEAR), reverse Monte Carlo (RMC) refinement, and hybrid reverse Monte Carlo (HRMC) refinement. The R_χ obtained by melt-quenching (MQ) using molecular dynamics with a cooling rate of 0.001 K/ps is shown for comparison. **(b)** Neutron pair distribution functions computed by FEAR, MQ, RMC, and HRMC. The data are compared with neutron diffraction data [44] **(c)** Final Wright's cost function R_χ offered by FEAR, MQ, RMC, and HRMC.

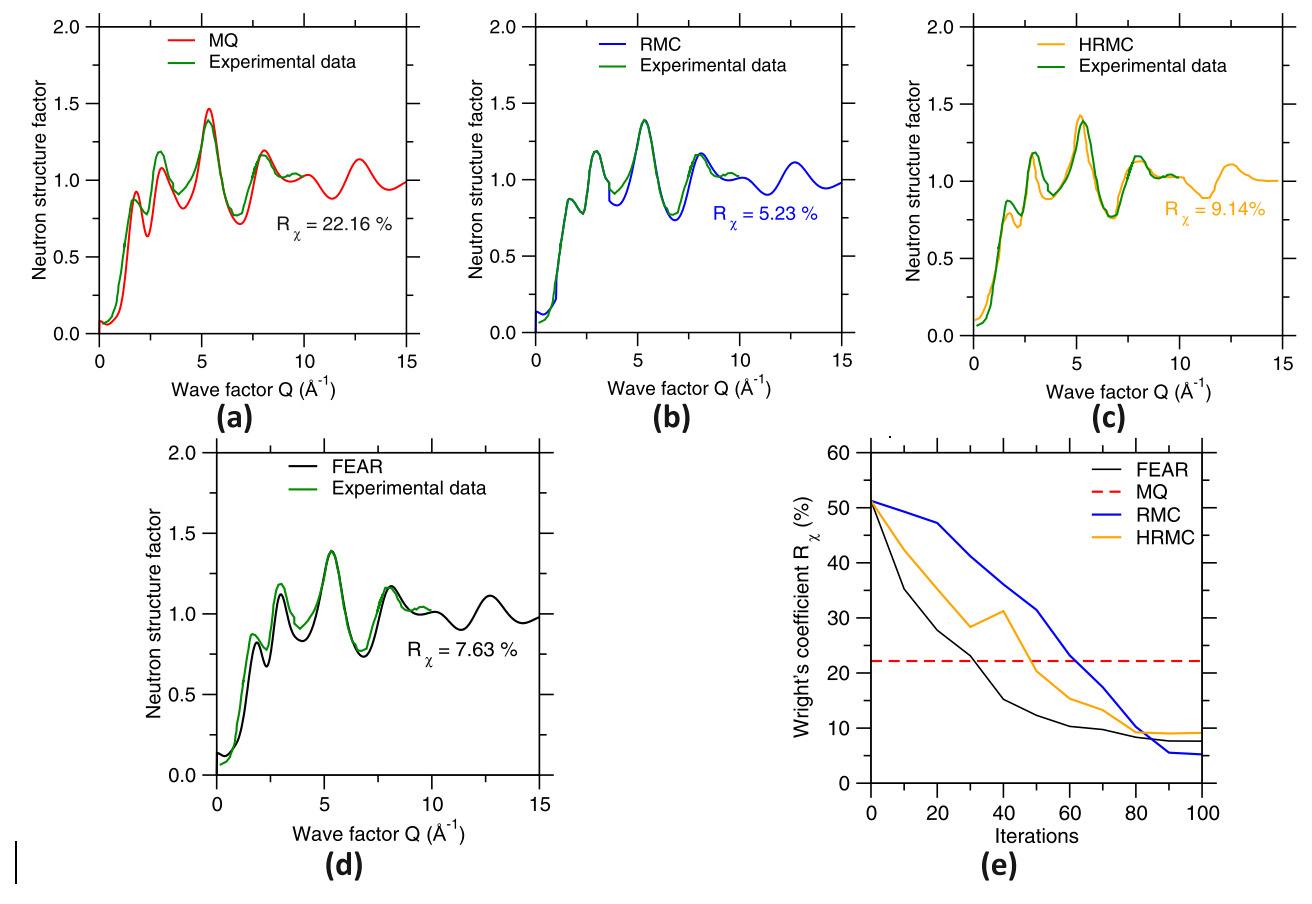


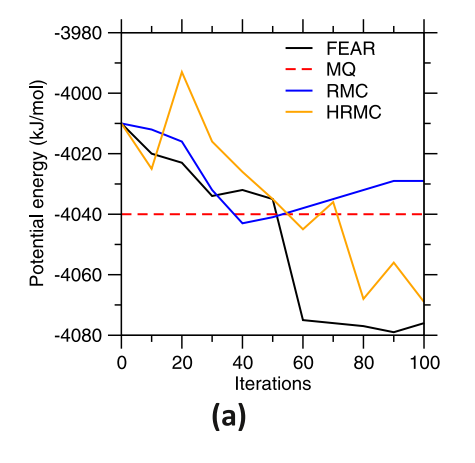
Fig. 5. Neutron structure factor computed by **(a)** melt-quenching (MQ) using molecular dynamics with a cooling rate of 0.001 K/ps, **(b)** reverse Monte Carlo (RMC) refinement, **(c)** hybrid reverse Monte Carlo (HRMC) refinement, and **(d)** force-enhanced atomic refinement (FEAR). The data are compared with experimental neutron diffraction data [41]. **(e)** Wright's coefficient R_χ (calculated for the structure factor) as a function of the iteration number upon FEAR, RMC, and HRMC refinement. The R_χ obtained by MQ with a cooling rate of 0.001 K/ps is shown for comparison.

for the structure factor) of 5.23%, 9.14%, and 7.63%, which is significantly improved as compared to that yielded by MD (i.e., 22.16%, see Fig. 5a). We note that, overall, HRMC offers the lowest level of accuracy—although an R_χ factor that is less than 10% is usually considered as acceptable. Again, we find that, although RMC eventually yields a lower R_χ factor than FEAR, RMC requires a few more iterations than FEAR to converge, which highlights again the high computational efficiency of FEAR refinement (see Fig. 5e).

We now focus on the thermodynamic stability of the configurations generated by FEAR, RMC, HRMC, and MQ-MD. Fig. 6 shows the evolution of the molar potential energy of the system upon RMC refinement. Overall, we find that RMC yields a potential energy that is

significantly higher (by more than 20 kJ/mol) than that offered by MQ-MD (see Fig. 6b). This result is not surprising since RMC is blind to the interatomic energy. Nevertheless, it highlights the fact that, although the configuration generated by RMC offers an excellent match with neutron diffraction data, the configuration generated by RMC is unstable and, hence, fairly unrealistic. This arises from the fact that, as mentioned above, many configurations (stable or not) can exhibit the same pair distribution function, which highlights the intrinsic limitations of RMC refinement.

In contrast, we observe that FEAR and HRMC both yield a potential energy that is significantly lower than that offered by MQ-MD (see Fig. 6a), in agreement with previous findings [29]. This is significant



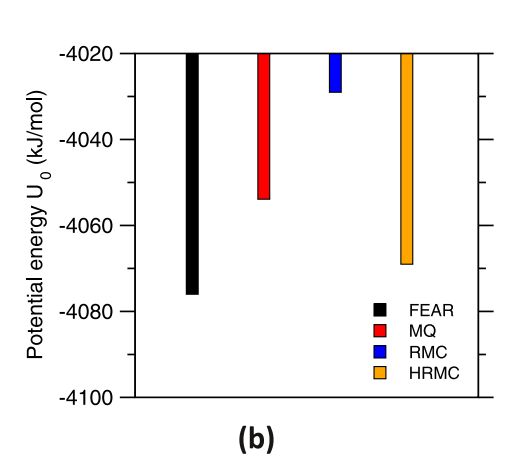


Fig. 6. (a) Molar potential energy as a function of the iteration number upon force-enhanced atomic refinement (FEAR), reverse Monte Carlo (RMC), and hybrid reverse Monte Carlo (HRMC) refinement. The energy obtained by melt-quenching (MQ) using molecular dynamics with a cooling rate of 0.001 K/ps is shown for comparison. (b) Final molar potential energy predicted by FEAR, MQ, RMC, and HRMC.

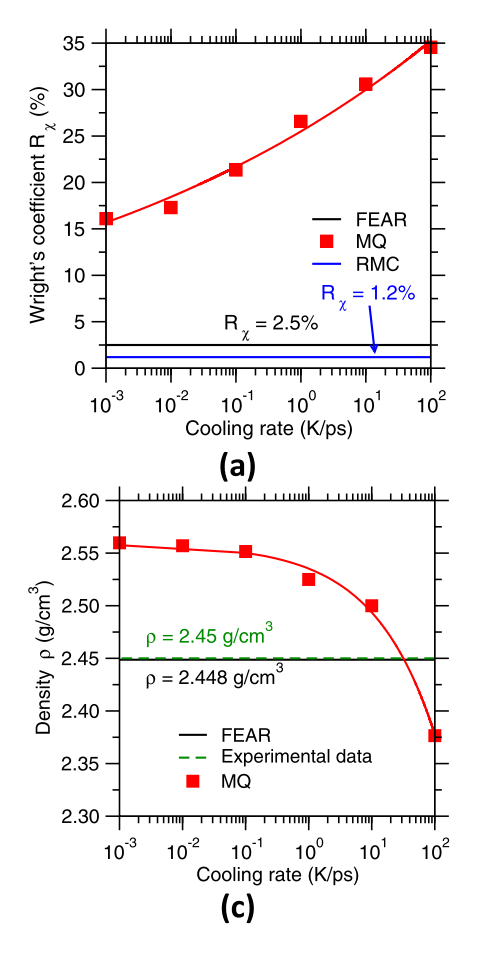
since it signals that, although FEAR, HRMC, and MQ-MD relies on the same interatomic forcefield, imposing a structural constraint (i.e., the neutron PDF) allows the structure to reach lower energy states. This suggests that, in the case of FEAR, the RMC refinement steps performed in between each energy minimization allow the system to jump over some large energy barriers and, thereby, reach some energy basins that would be inaccessible during the limited timescales of MD simulations. Although both FEAR and HRMC eventually yield a low energy, we note that FEAR refinement eventually results in a more stable configuration. In addition, we observe that HRMC is slower to converge than FEAR and exhibits more fluctuations. It is also worth pointing out that, since the energy needs to be calculated at each Monte Carlo step, HRMC is significantly less computationally efficient than FEAR. Overall, these results demonstrate that FEAR refinement can generate some glass structures that simultaneously exhibit unprecedented level of agreement with experimental data and energetic stability.

Since FEAR systematically outperforms HRMC, we solely focus on comparing FEAR, RMC, and MQ-MD in the following of this investigation. To further appreciate the magnitude of the variations in R_{γ} and potential energy yielded by FEAR and RMC, we compare them to the variations resulting from the use of different cooling rates in MQ-MD simulations. Fig. 7a first shows the evolution of R_{χ} as a function of a function of the cooling rate (as computed from the MQ-MD simulations). As expected, we find that R_{γ} decreases upon decreasing cooling rate [9], which indicates that the PDF of the glass structures generated by MQ-MD gradually converges toward the experimental neutron diffraction data as the cooling rate decreases. Nevertheless, independently of the cooling rate, the R_{χ} coefficient of the glass structures simulated by MQ-MD systematically remains significantly higher than those obtained by RMC and FEAR. Based on cooling-rate dependence predicted by mode-coupling theory [52], the R_{χ} are fitted by a power law and extrapolated to lower cooling rates. Notably, this rough extrapolation of

the MD-derived R_χ coefficients as a function of the cooling rate (assuming a power law dependence, see Fig. 7a [9,52]) suggests that a cooling rate of about 100 K/s (i.e., 10^{-10} K/ps, which is fairly comparable to experimental cooling rates) would be needed for a melt-quench MD simulation to yield a R_χ coefficient that is comparable to that offered by FEAR. Such a simulation would roughly require a CPU time of 100 million years to complete. This highlights the clear advantage of FEAR refinement over conventional melt-quenching MD simulations.

Fig. 7b shows the evolution of the molar potential energy of the MD-based simulated glasses as a function of the cooling rate. As expected, the potential energy decreases upon decreasing cooling rate [9], which indicates that the system becomes more stable and reaches deeper states within the energy landscape (or achieves lower fictive temperatures) [53,54]. We note that the potential energy offered by RMC is significantly higher than that offered by MQ-MD, even for a very high cooling rate of 100 K/ps. In turn, we find that the magnitude of the decrease in potential energy provided by FEAR as compared to a 0.001 K/ps MQ-MD simulation (i.e., about 20 kJ/mol) is comparable to that observed upon a variation of 5 orders of magnitude of the cooling rate (i.e., from 100 to 0.001 K/ps, see Fig. 7b).

Finally, we focus on the evolution of glass density. As shown in Fig. 7c, the glass density predicted by MQ-MD simulations expectedly tends to increase upon decreasing cooling rate. This echoes the fact that glasses usually become more compact upon slower cooling rate (with the notable exception of pure silica) [14,54]. However, as the cooling rate decreases, we note that MQ-MD simulations tend to overestimate the density of sodium silicate observed experimentally, i.e., 2.45 g/cm³ [47,55]. The origin of this discrepancy is unclear and might be a spurious effect of the melt-quenching procedure (for instance, the empirical forcefield used herein may not be accurate at high-temperature, i.e., when the atoms are far from equilibrium). In contrast, we find that



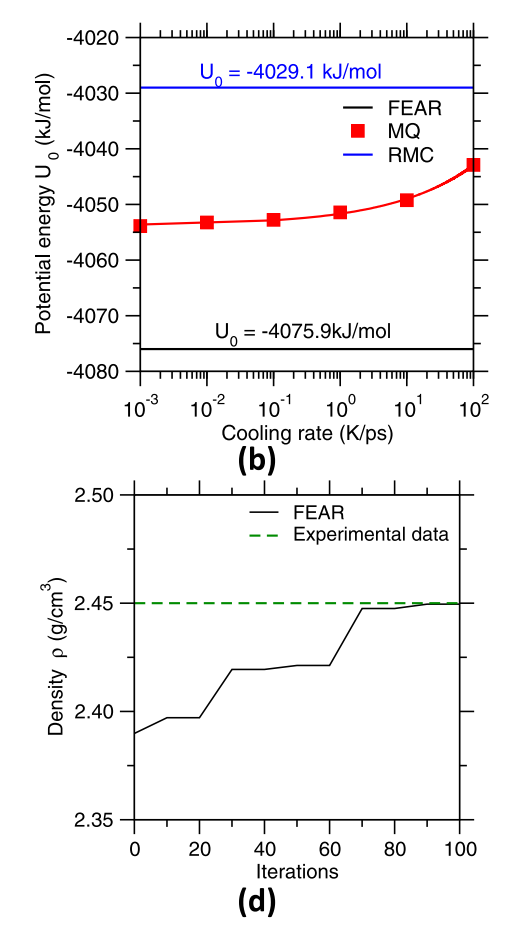


Fig. 7. (a) Wright's coefficient R_{χ^2} **(b)** molar potential energy, and **(c)** density predicted by melt-quenching (MQ) molecular dynamics simulations as a function of the cooling rate. The lines are to guide the eye. The values yielded by force-enhanced atomic refinement (FEAR) and reverse Monte Carlo (RMC) are added for comparison. **(d)** Density as a function of the iteration number upon FEAR refinement. The density values in panels (c) and (d) are compared with the experimental data [47,55].

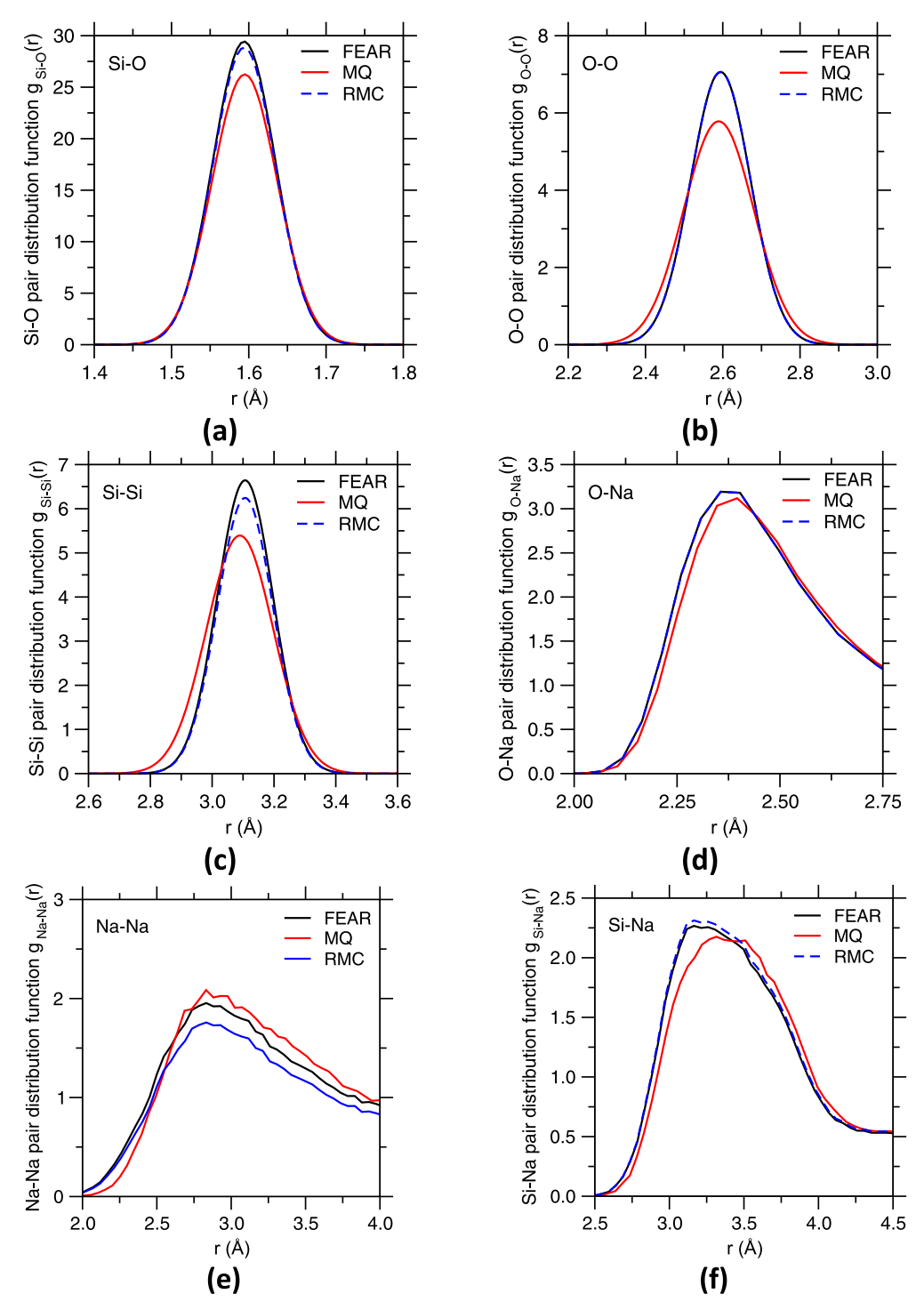
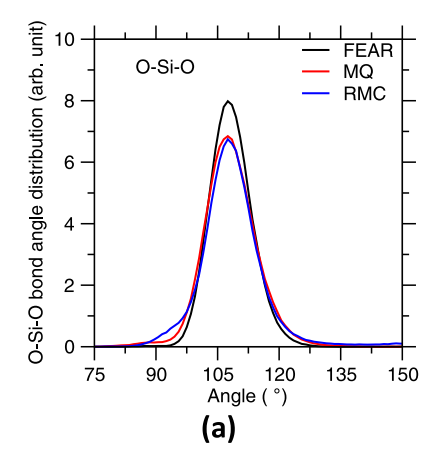


Fig. 8. (a) Si-O, (b) O-O, (c) Si-Si, (d) O-Na, (e) N-Na, and (f) Si-Na partial pair distribution functions computed by force-enhanced atomic refinement (FEAR), melt-quenching (MQ) molecular dynamics, and reverse Monte Carlo (RMC).

FEAR yields a glass density that shows an excellent match with experimental data (see Fig. 7d). This suggests that the fact that the MQ-MD simulation overestimates the glass density is not simply limitation of the empirical forcefield (at room temperature). Note that, in the pure RMC simulations, the density is fixed to be equal to the experimental value—so that RMC simulations cannot be used to predict the glass density. Again, these results suggest that the combination of energy minimization and experimental constraints can overcome the limitations of MQ-MD and RMC simulations.

3.3. Short-range order signatures of the force-enhanced refinement

We now explore how the level of improvement offered by FEAR refinement (in terms of R_χ and energetic stability) manifests itself in the short-range order (<3 Å) structure of the simulated sodium silicate glass. Fig. 8 shows all the partial PDFs obtained by MQ-MD, RMC, and FEAR. We first note that the positions of the Si–O and O–O peaks around 1.6 and 2.6 Å, respectively, remain fairly unaffected, although FEAR and RMC appear to predict a sharper peak, that is, a more ordered local environment for Si atoms (see Figs. 8a and b). In contrast, we note the Si–Si peak around 3.1 Å predicted by FEAR and RMC shifts toward



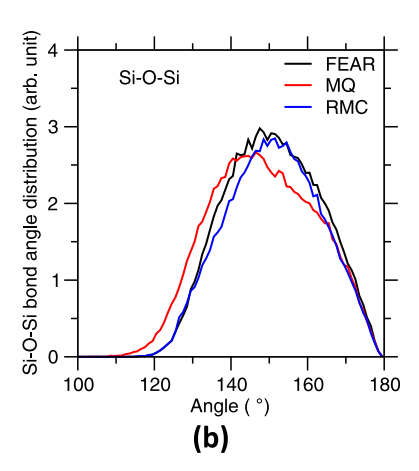


Fig. 9. (a) O–Si–O and (b) Si–O–Si partial bond angle distributions computed by force-enhanced atomic refinement (FEAR), melt-quenching (MQ) molecular dynamics, and reverse Monte Carlo (RMC).

higher distances compared to MQ-MD (see Fig. 8c). This behavior echoes the peak shift observed upon decreasing cooling rate in MQ-MD simulations [9]. The fact that the average Si–Si distance increases upon FEAR refinement while the Si–O bond distance remains constant suggests an opening of the Si–O–Si angle (see below). We then note that the Na–O PDF remains largely unaffected (see Fig. 8d), which suggests that what the local environment of the Na atoms only weakly depends on the simulation technique that is used. More significant variations are observed in the Na–Na PDF (see Fig. 8e). Specifically, we find that the peak intensity predicted by RMC is lower than those offered by MQ-MD and FEAR, which suggests that RMC underestimates the degree of modifier clustering [9]. Finally, we note that both FEAR and RMC simulations predict a Si–Na PDF that is more asymmetric than that predicted by MO-MD (see Fig. 8f).

Then we direct our attention to the angular environment of each element. Fig. 9 shows the O-Si-O (intratetrahedral) and Si-O-Si (intertetrahedral) partial bond angle distributions (PBADs) offered by FEAR, MD, and RMC. First, we note that the average O-Si-O angle remains unaffected, with a PBAD centered around 109°, which is in agreement with the tetrahedral environment of the Si atoms. However, we observe that the O-Si-O PBAD becomes sharper upon FEAR refinement, which denotes the existence of a more ordered angular environment for the Si atoms. This echoes the fact that the O-Si-O PBAD computed by MD simulations also becomes sharper upon decreasing cooling rate [9]. Second, we observe that the Si-O-Si PBAD becomes sharper and shifts toward higher angle values upon FEAR refinement. The behavior is supported by RMC simulations and denotes an opening of the intertetrahedral angle. This also echoes the fact that the average Si-O-Si angle computed by MD simulations increases upon decreasing cooling rate [9]. Overall, this suggests that more relaxed glassy silicate structures are associated with more open intertetrahedral angles [9].

3.4. Topological signatures of the force-enhanced refinement

We now investigate the variation in network connectivity upon refinement. Although FEAR, MD, and RMC yield similar coordination numbers (e.g., 4 for Si) and fraction of non-bridging oxygen (NBO, i.e., each Na creates 1 NBO), we observe some variations in the interconnectivity of the SiO₄ tetrahedral polytopes. Such connectivity is captured by the Q_n distribution, wherein a Q_n species denotes an SiO₄ tetrahedral unit that is connected to n other Si atoms and, hence, that comprises 4-n NBOs.

Due to the high cooling rates they rely on, melt-quenching MD simulations typically yield glass structures that are more disordered than those observed experimentally [13]. Consequently, MD simulations tend to predict glass structures wherein the NBO are more randomly attached to the Si atoms. As such, MD simulations typically yield Q_n distributions that agree well with the predictions from a random model [21,31,56], but, in turn, do not match with experimental data [57]. Although lower cooling rates tend to improve the agreement between MD simulations and experimental data [9], we observe that, even with a slow cooling rate of 0.001 K/ps (as used herein), MD simulations yield a fairly random Q_n distribution. Such randomness manifests itself by the fact that MD (i) underestimates the fraction of Q_3 units and (ii) overestimates the fraction of Q_0 defects (see Ref. [9]).

As shown in Fig. 10, FEAR refinement partially addresses these two points. First, both FEAR and RMC yield a significantly lower fraction of Q_0 defects—and such units virtually disappear upon FEAR refinement (see Fig. 10b), in agreement with experimental data [9]. Second, we find that, although RMC predicts a fraction of Q_3 units that is

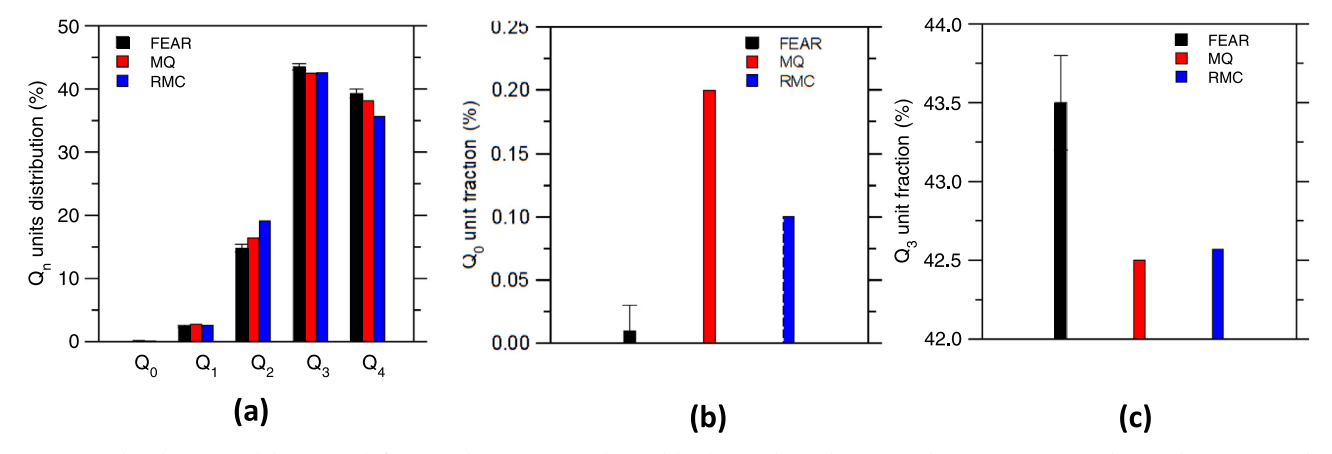


Fig. 10. (a) Q_n distribution, and fractions of (b) Q_0 and (c) Q_3 units obtained by force-enhanced atomic refinement (FEAR), melt-quenching (MQ) molecular dynamics, and reverse Monte Carlo (RMC).

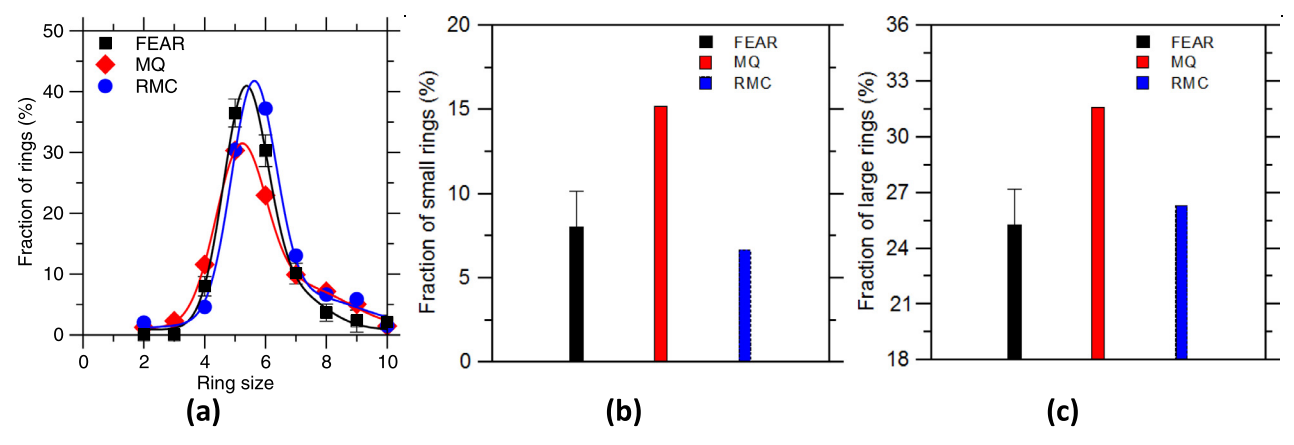


Fig. 11. (a) Ring size distribution for FEAR, MQ and RMC, respectively. (b) Small ring size (< 5) and (c) Large ring size (>6) distribution for FEAR, MQ and RMC, respectively.

comparable to MD, FEAR yields an increased fraction of Q_3 units. The preferential formation of Q_3 units is also observed in MD simulations upon decreasing cooling rate [9] and has been explained by the fact that such units are isostatic and exhibit minimum internal stress [58]. Overall, this shows that FEAR yields a glass topology that is more ordered (i.e., less random) than those predicted by MD and RMC.

3.5. Medium-range order signatures of the force-enhanced refinement

Finally, we investigate how FEAR refinement manifests itself in the medium-range order structure of the simulated sodium silicate glass. In disordered silicate systems, the medium-range order is primarily captured by the ring size distribution—wherein silicate rings are defined as the shortest closed paths made of Si—O bonds within the atomic network [59]. Here, the ring size distribution of each configuration is computed by using the RINGS package [60].

Fig. 11 shows that ring size distribution computed by FEAR, MD, and RMC. We first note that the ring size distribution offered by MD is in agreement with previous works, being centered around 5-to-6membered rings [10,43]—wherein the ring size is expressed in terms of the number of Si atoms it comprises [61]. Interestingly, we then observe that both FEAR and RMC yield a sharper ring size distribution than that predicted by MD (see Fig. 11a). Specifically, both FEAR and RMC predict a lower fraction of small rings (i.e., 4-membered and smaller, see Fig. 11b). In particular, 2-membered (i.e., edge-sharing units) and 3-membered rings are virtually absent from the glass structure after FEAR refinement. Similarly, both FEAR and RMC predict a lower fraction of larger rings (i.e., 7-membered and larger, see Fig. 11c). In turn, both FEAR and RMC predict a higher fraction of 6membered rings than MD. These results echo the fact that the fractions of both small and large rings predicted by MD tend to decrease upon decreasing cooling rate [43]. This is also in agreement with the fact that small rings are over-constrained and, hence, experience some internal stress [43,59]. Overall, these results suggest that, when properly relaxed, sodium silicate glasses exhibit a more ordered medium-range order structure (i.e., sharper ring size distribution) than suggested by MD simulations.

6. Conclusions

Overall, FEAR refinement yields a sodium silicate glass structure that simultaneously exhibits enhanced agreement with diffraction data and higher energetic stability as compared to configurations generated by MD, RMC, or HRMC. As such, FEAR offers an unprecedented description of the atomic structure of sodium silicate glasses. We find that the enhanced thermodynamic stability offered by FEAR primarily finds its roots in the Q_n and ring size distributions of the network. Our

findings thus suggest that the structure of silicate glasses is more ordered, less random than previously suggested by MD simulations. Overall, this study establishes FEAR as a promising tool to explore the complex, largely hidden atomic structure of disordered solids.

CRediT authorship contribution statement

Qi Zhou: Conceptualization, Methodology, Investigation, Writing - original draft, Writing - review & editing. Tao Du: Methodology, Software, Validation. Lijie Guo: Supervision, Funding acquisition, Writing - review & editing. Morten M. Smedskjaer: Writing - review & editing, Supervision. Mathieu Bauchy: Conceptualization, Resources, Writing - original draft, Writing - review & editing, Supervision, Project administration, Funding acquisition.

Declaration of Competing Interest

The authors declare that they have no known competing financial interests or personal relationships that could have appeared to influence the work reported in this paper.

Acknowledgements

The authors acknowledge financial support for this research provided by the National Science Foundation under Grant No. 1928538 and the International Cooperation on Scientific and Technological Innovation Programsof BGRIMM under Grant No. 2017YFE0107000. M.M.S. acknowledges funding from the Independent Research Fund Denmark (Grant No. 7017-00019).

Supplementary materials

Supplementary material associated with this article can be found, in the online version, at doi:10.1016/j.jnoncrysol.2020.120006.

References

- [1] D.L. Morse, J.W. Evenson, Welcome to the Glass Age, Int. J. Appl. Glass Sci. 7 (2016) 409–412, https://doi.org/10.1111/ijag.12242.
- [2] J.C. Mauro, Decoding the glass genome, Curr. Opin. Solid State Mater. Sci. 22 (2018) 58-64, https://doi.org/10.1016/j.cossms.2017.09.001.
- [3] J.C. Mauro, Grand challenges in glass science, Front. Mater. 1 (2014) 20, https://doi.org/10.3389/fmats.2014.00020.
- [4] J.C. Mauro, E.D. Zanotto, Two centuries of glass research: historical trends, current status, and grand challenges for the future, Int. J. Appl. Glass Sci. 5 (2014) 313–327, https://doi.org/10.1111/jiag.12087.
- [5] J.C. Mauro, C.S. Philip, D.J. Vaughn, M.S. Pambianchi, Glass science in the united states: current status and future directions, Int. J. Appl. Glass Sci. 5 (2014) 2–15, https://doi.org/10.1111/ijag.12058.
- [6] P. Biswas, R. Atta-Fynn, D.A. Drabold, Reverse Monte Carlo modeling of amorphous

- silicon, Phys. Rev. B. (2004) 69, https://doi.org/10.1103/PhysRevB.69.195207.
- [7] A. Pandey, P. Biswas, D.A. Drabold, Inversion of diffraction data for amorphous materials, Sci. Rep. 6 (2016) 33731, https://doi.org/10.1038/srep33731.
- [8] M. Bauchy, Structural, vibrational, and elastic properties of a calcium aluminosilicate glass from molecular dynamics simulations: the role of the potential, J. Chem. Phys. 141 (2014) 024507, https://doi.org/10.1063/1.4886421.
- [9] X. Li, W. Song, K. Yang, N.M.A. Krishnan, B. Wang, M.M. Smedskjaer, J.C. Mauro, G. Sant, M. Balonis, M. Bauchy, Cooling rate effects in sodium silicate glasses: bridging the gap between molecular dynamics simulations and experiments, J. Chem. Phys. 147 (2017) 074501, https://doi.org/10.1063/1.4998611.
- [10] J. Du, A.N. Cormack, The medium range structure of sodium silicate glasses: a molecular dynamics simulation, J. Non-Cryst. Solids. 349 (2004) 66–79, https://doi.org/10.1016/j.jnoncrysol.2004.08.264.
- [11] C. Massobrio, J. Du, M. Bernasconi, P.S. Salmon (Eds.), Molecular Dynamics Simulations of Disordered Materials, Springer International Publishing, Cham, 2015, https://doi.org/10.1007/978-3-319-15675-0.
- [12] J. Du, Challenges in molecular dynamics simulations of multicomponent oxide glasses, in: C. Massobrio, J. Du, M. Bernasconi, P.S. Salmon (Eds.), Mol. Dyn. Simul. Disord. Mater. Springer International Publishing, 2015, pp. 157–180.
- [13] L. Huang, J. Kieffer, Challenges in modeling mixed ionic-covalent glass formers, in: C. Massobrio, J. Du, M. Bernasconi, P.S. Salmon (Eds.), Mol. Dyn. Simul. Disord. Mater. Springer International Publishing, 2015, pp. 87–112, https://doi.org/10.1007/978-3-319-15675-0 4.
- [14] Z. Liu, Y. Hu, X. Li, W. Song, S. Goyal, M. Micoulaut, M. Bauchy, Glass relaxation and hysteresis of the glass transition by molecular dynamics simulations, Phys. Rev. B. 98 (2018) 104205, https://doi.org/10.1103/PhysRevB.98.104205.
- [15] K. Vollmayr, W. Kob, K. Binder, Cooling-rate effects in amorphous silica: a computer-simulation study, Phys. Rev. B. 54 (1996) 15808–15827, https://doi.org/10.1103/PhysRevB.54.15808.
- [16] K. Vollmayr, W. Kob, K. Binder, How do the properties of a glass depend on the cooling rate? A computer simulation study of a Lennard-Jones system, J. Chem. Phys. (1998), https://doi.org/10.1063/1.472326.
- [17] A.E. Geissberger, F.L. Galeener, Raman studies of vitreous SIO₂ versus fictive temperature, Phys. Rev. B. 28 (1983) 3266–3271, https://doi.org/10.1103/ PhysRevB.28.3266.
- [18] J.C. Mauro, R.J. Loucks, Forbidden glasses and the failure of fictive temperature, J. Non-Cryst. Solids. 355 (2009) 676–680, https://doi.org/10.1016/j.jnoncrysol. 2008 11 025
- [19] M.M. Smedskjaer, M. Bauchy, J.C. Mauro, S.J. Rzoska, M. Bockowski, Unique effects of thermal and pressure histories on glass hardness: structural and topological origin, J. Chem. Phys. 143 (2015) 164505, https://doi.org/10.1063/1.4934540.
- [20] M. Wang, B. Wang, T.K. Bechgaard, J.C. Mauro, S.J. Rzoska, M. Bockowski, M.M. Smedskjaer, M. Bauchy, Crucial effect of angular flexibility on the fracture toughness and nano-ductility of aluminosilicate glasses, J. Non-Cryst. Solids. 454 (2016) 46–51. https://doi.org/10.1016/j.ipongrysol.2016.10.020
- (2016) 46–51, https://doi.org/10.1016/j.jnoncrysol.2016.10.020.
 [21] L. Adkins, A. Cormack, Large-scale simulations of sodium silicate glasses, J. Non-Cryst. Solids. 357 (2011) 2538–2541, https://doi.org/10.1016/j.jnoncrysol.2011.03.012
- [22] R.L. McGreevy, Reverse Monte Carlo modelling, J. Phys. Condens. Matter. 13 (2001) R877–R913, https://doi.org/10.1088/0953-8984/13/46/201.
- [23] R.L. McGreevy, L. Pusztai, Reverse Monte Carlo simulation: a new technique for the determination of disordered structures, Mol. Simul. 1 (1988) 359–367, https://doi. org/10.1080/08927028808080958
- [24] C.R. Müller, V. Kathriarachchi, M. Schuch, P. Maass, V.G. Petkov, Reverse Monte Carlo modeling of ion conducting network glasses: an evaluation based on molecular dynamics simulations, Phys. Chem. Chem. Phys. 12 (2010) 10444, https:// doi.org/10.1039/c003472i.
- [25] D.A. Drabold, Topics in the theory of amorphous materials, Eur. Phys. J. B. 68 (2009) 1–21, https://doi.org/10.1140/epjb/e2009-00080-0.
- [26] G. Opletal, T. Petersen, B. O'Malley, I. Snook, D.G. McCulloch, N.A. Marks, I. Yarovsky, Hybrid approach for generating realistic amorphous carbon structure using metropolis and reverse Monte Carlo, Mol. Simul. 28 (2002) 927–938, https:// doi.org/10.1080/089270204000002584.
- [27] C. Bousige, A. Boţan, F.-J. Ulm, R.J.-M. Pellenq, B. Coasne, Optimized molecular reconstruction procedure combining hybrid reverse Monte Carlo and molecular dynamics, J. Chem. Phys. 142 (2015) 114112, https://doi.org/10.1063/1. 4914921.
- [28] S.K. Jain, R.J.-M. Pellenq, J.P. Pikunic, K.E. Gubbins, Molecular modeling of porous carbons using the hybrid reverse Monte Carlo method, Langmuir 22 (2006) 9942–9948, https://doi.org/10.1021/la053402z.
- [29] A. Pandey, P. Biswas, D.A. Drabold, Force-enhanced atomic refinement: structural modeling with interatomic forces in a reverse Monte Carlo approach applied to amorphous Si and SiO₂, Phys. Rev. B. (2015) 92, https://doi.org/10.1103/ PhysRevB. 92. 155205.
- [30] A. Pandey, P. Biswas, B. Bhattarai, D.A. Drabold, Realistic inversion of diffraction data for an amorphous solid: the case of amorphous silicon, Phys. Rev. B. 94 (2016) 235208, https://doi.org/10.1103/PhysRevB.94.235208.
- [31] M. Bauchy, Structural, vibrational, and thermal properties of densified silicates: insights from molecular dynamics, J. Chem. Phys. 137 (2012) 044510, https://doi. org/10.1063/1.4738501.
- [32] J. Horbach, W. Kob, K. Binder, C.A. Angell, Finite size effects in simulations of glass dynamics, Phys. Rev. E. 54 (1996) R5897–R5900, https://doi.org/10.1103/

- PhysRevE.54.R5897.
- [33] M. Bauchy, M. Micoulaut, From pockets to channels: density-controlled diffusion in sodium silicates, Phys. Rev. B. 83 (2011) 184118, https://doi.org/10.1103/ PhysRevB.83.184118.
- [34] M. Bauchy, B. Guillot, M. Micoulaut, N. Sator, Viscosity and viscosity anomalies of model silicates and magmas: a numerical investigation, Chem. Geol. 346 (2013) 47–56, https://doi.org/10.1016/j.chemgeo.2012.08.035.
- [35] Y. Yu, B. Wang, Y.J. Lee, M. Bauchy, Fracture toughness of silicate glasses: insights from molecular dynamics simulations, Symp. UU – Struct.-Prop. Relat. Amorph. Solids, 2015, https://doi.org/10.1557/opl.2015.50.
- [36] B. Wang, Y. Yu, M. Wang, J.C. Mauro, M. Bauchy, Nanoductility in silicate glasses is driven by topological heterogeneity, Phys. Rev. B. 93 (2016) 064202, https://doi. org/10.1103/PhysRevB.93.064202.
- [37] B. Wang, Y. Yu, Y.J. Lee, M. Bauchy, Intrinsic Nano-Ductility of glasses: the critical role of composition, Front. Mater. 2 (2015) 11, https://doi.org/10.3389/fmats. 2015.00011.
- [38] M. Bauchy, M. Micoulaut, Densified network glasses and liquids with thermodynamically reversible and structurally adaptive behaviour, Nat. Commun. 6 (2015) 6398, https://doi.org/10.1038/ncomms7398.
- [39] B. Mantisi, M. Bauchy, M. Micoulaut, Cycling through the glass transition: evidence for reversibility windows and dynamic anomalies, Phys. Rev. B. 92 (2015) 134201, https://doi.org/10.1103/PhysRevB.92.134201.
- [40] M. Bauchy, B. Wang, M. Wang, Y. Yu, M.J. Abdolhosseini Qomi, M.M. Smedskjaer, C. Bichara, F.-J. Ulm, R. Pellenq, Fracture toughness anomalies: viewpoint of topological constraint theory, Acta Mater 121 (2016) 234–239, https://doi.org/10. 1016/j.actamat.2016.09.004.
- [41] R.W. Hockney, J.W. Eastwood, Computer Simulation Using Particles, Taylor & Francis Group, New York, NY, 1988. https://www.google.com/books/edition/Computer Simulation_Using_Particles/nTOFkmnCQuIC?hl = en&gbpv = 0
- [42] S. Plimpton, Fast parallel algorithms for short-range molecular dynamics, J. Comput. Phys. 117 (1) (1995) 1–19.
- [43] W. Song, X. Li, B. Wang, N.M. Anoop Krishnan, S. Goyal, M.M. Smedskjaer, J.C. Mauro, C.G. Hoover, M. Bauchy, Atomic picture of structural relaxation in silicate glasses, Appl. Phys. Lett. 114 (2019) 233703, https://doi.org/10.1063/1. 5095529
- [44] A.C. Wright, A.G. Clare, B. Bachra, R.N. Sinclair, A.C. Hannon, B. Vessal, Neutron diffraction studies of silicate glasses, Trans. Am. Crystallogr. Assoc. 27 (1991) 239–254.
- [45] V.F. Sears, Neutron scattering lengths and cross sections, Neutron News 3 (1992) 26–37, https://doi.org/10.1080/10448639208218770.
- [46] A.C. Wright, The comparison of molecular dynamics simulations with diffraction experiments, J. Non-Cryst. Solids. 159 (1993) 264–268, https://doi.org/10.1016/ 0022-3093(93)90232-M.
- [47] Y. Vaills, T. Qu, M. Micoulaut, F. Chaimbault, P. Boolchand, Direct evidence of rigidity loss and self-organization in silicate glasses, J. Phys. Condens. Matter. 17 (2005) 4889–4896, https://doi.org/10.1088/0953-8984/17/32/003.
- [48] Y. Yu, M. Wang, D. Zhang, B. Wang, G. Sant, M. Bauchy, Stretched exponential relaxation of glasses at low temperature, Phys. Rev. Lett. 115 (2015) 165901, https://doi.org/10.1103/PhysRevLett.115.165901.
- [49] Y. Yu, M. Wang, M.M. Smedskjaer, J.C. Mauro, G. Sant, M. Bauchy, Thermometer effect: origin of the mixed alkali effect in glass relaxation, Phys. Rev. Lett. 119 (2017) 095501, https://doi.org/10.1103/PhysRevLett.119.095501.
- [50] H. Jabraoui, E.M. Achhal, A. Hasnaoui, J.-L. Garden, Y. Vaills, S. Ouaskit, Molecular dynamics simulation of thermodynamic and structural properties of silicate glass: effect of the alkali oxide modifiers, J. Non-Cryst. Solids. 448 (2016) 16–26, https://doi.org/10.1016/j.jnoncrysol.2016.06.030.
- [51] C. Huang, A.N. Cormack, The structure of sodium silicate glass, J. Chem. Phys. 93 (1990) 8180–8186, https://doi.org/10.1063/1.459296.
- [52] W. Kob, H.C. Andersen, Testing mode-coupling theory for a supercooled binary Lennard-Jones mixture I: the van Hove correlation function, Phys. Rev. E. 51 (1995) 4626–4641, https://doi.org/10.1103/PhysRevE.51.4626.
- [53] P.G. Debenedetti, F.H. Stillinger, Supercooled liquids and the glass transition, Nature 410 (2001) 259–267, https://doi.org/10.1038/35065704.
- [54] A.K. Varshneya, Fundamentals of Inorganic Glasses, Academic Press Inc, 1993.
 [55] N.P. Bansal, R.H. Doremus, Handbook of Glass Properties, Elsevier, 2013.
- [56] J. Horbach, W. Kob, Structure and dynamics of sodium disilicate, Philos. Mag. B-Phys. Condens. Matter Stat. Mech. Electron. Opt. Magn. Prop. 79 (1999) 1981–1986, https://doi.org/10.1080/13642819908223085.
- [57] H. Maekawa, T. Maekawa, K. Kawamura, T. Yokokawa, The structural groups of alkali silicate glasses determined from 29Si MAS-NMR, J. Non-Cryst. Solids. 127 (1991) 53–64, https://doi.org/10.1016/0022-3093(91)90400-Z.
- [58] X. Li, W. Song, M.M. Smedskjaer, J.C. Mauro, M. Bauchy, Quantifying the internal stress in over-constrained glasses by molecular dynamics simulations, J. Non-Cryst. Solids X. 1 (2019) 100013, https://doi.org/10.1016/j.nocx.2019.100013.
- [59] M. Micoulaut, J.C. Phillips, Rings and rigidity transitions in network glasses, Phys. Rev. B. 67 (2003) 104204, https://doi.org/10.1103/PhysRevB.67.104204.
- [60] S. Le Roux, P. Jund, Ring statistics analysis of topological networks: new approach and application to amorphous GeS2 and SiO2 systems, Comput. Mater. Sci. 49 (2010) 70–83, https://doi.org/10.1016/j.commatsci.2010.04.023.
- [61] S.K. Sharma, J.F. Mammone, M.F. Nicol, Raman investigation of ring configurations in vitreous silica, Nature 292 (1981) 140–141, https://doi.org/10.1038/292140a0.